THE ASTROPHYSICAL JOURNAL, 545:807–812, 2000 December 20

LIGHT CURVES OF GAMMA-RAY BURST OPTICAL FLASHES

SHIHO KOBAYASHI
Department of Earth and Space Science, Osaka University, Toyonaka 560, Japan
Received 2000 June 2; accepted 2000 July 26

ABSTRACT

The standard model of gamma-ray burst (GRB) afterglows assumes that relativistically expanding material is decelerating as a result of interaction with the surrounding medium. The afterglows are well described by the synchrotron radiation from a forward shock, while the strong optical flash associated with GRB 990123 can be attributed to the emission from a reverse shock. We give a detailed study on the reverse shock emission. The full light curves are calculated for long and short GRB cases. We discuss the lack of the prompt optical detections by ROTSE for GRB 981121 and GRB 981223.

Subject headings: gamma rays: bursts — hydrodynamics — relativity — shock waves

1. INTRODUCTION

The gamma-ray burst (GRB) afterglow is believed to involve a relativistically expanding fireball. The interstellar matter (ISM) influences the fireball shell after it has been collected enough and the considerable energy has been transferred from the shell to the ISM. The energy transfer is due to two shocks: a forward shock propagating into the ISM and a reverse shock propagating into the shell.

The afterglow observations are fairly well described by the synchrotron emission from the ISM electrons accelerated by the forward shock; it is considered as a confirmation of the relativistic fireball. However, the current afterglow observations detect the radiation from several hours after the GRBs. At this stage, the Lorentz factor of the forward shock is not ultrarelativistic, less than ~ 10. Furthermore, the dynamics depends only on two parameters: the explosion energy and the ISM density. The afterglow observations provide neither verification of the extreme relativistic motion nor the properties of the fireball, which can constrain models of the GRB source.

The counterpart of the afterglow, the emission from a reverse shock, was also predicted (Mészaros & Rees 1997; Sari & Piran 1999a). When a reverse shock crosses a shell, the forward-shocked ISM and the reverse-shocked shell carry comparable amounts of energy. However, the typical temperature of the shocked shell is lower since the mass density of the shell is higher. Consequently, the typical frequency from the shocked shell is lower. A prompt optical emission from GRB 990123 (Akerlof et al. 1999) can be considered as this emission (Sari & Piran 1999b; Kobayashi & Sari 2000).

The emission from the reverse shock is sensitive to the properties of the fireball. The observations can provide some important clues on the nature of the GRB source. Previous studies (Sari & Piran 1999a, 1999b) focused on the emission at the peak time. In this paper we calculate the full light curves for several frequency regimes. In § 2 we discuss the hydrodynamics of the relativistic fireballs on which the light curves highly depend. In § 3 we calculate the light curves for a long burst and a short burst case. We compare our estimates with the ROTSE observations in § 4. We first show that the initial parameters of the fireball can be determined by the observations for GRB 990123, and then we make some comments on the lack of the prompt detections by ROTSE for GRB 981121 and GRB 981223. In § 5 we give conclusions.

2. HYDRODYNAMICS OF A RELATIVISTIC SHELL

Consider a relativistic shell with an energy E, a Lorentz factor η, and a width in laboratory frame Δ_0 expanding into the ISM with a particle number density n_1. When the shell sweeps a large volume of the ISM, it begins to be decelerated. The interaction between the shell and the ISM is described by two shocks: a forward shock propagating into the ISM and a reverse shock propagating into the shell. There are four regions separated by the two shocks: (1) the ISM, (2) the shocked ISM, (3) the shocked shell material, and (4) the unshocked shell material. Using the jump conditions for the shocks and the equality of pressure and velocity along the contact discontinuity, we can estimate the Lorentz factor γ, the pressure p, and the number density n in the shocked regions as functions of three variables: n_1, n_4, and η (Blandford & McKee 1976).

There are two limits to get a simple analytic solution (Sari & Piran 1995). If the shell density is high ($n_4 \gg \eta^2 n_1$), the reverse shock is Newtonian, which means that the Lorentz factor of the shocked shell material $\bar{\gamma}_3$ is almost unity in frame of the unshocked shell material. It is too weak to slow down the shell effectively ($\gamma_3 \sim \eta$). On the other hand, if the density is low ($n_4 \ll \eta^2 n_1$), the reverse shock is relativistic [$\bar{\gamma}_3 \sim (n_1/n_4)^{1/4}(\eta/2)^{1/2} \gg 1$] and it considerably decelerates the shell material [$\gamma_3 \sim (n_4/n_1)^{1/4}(\eta/2)^{1/2} \ll \eta$]. Once γ_3 is determined, the density and the pressure in the shocked shell region are given by $n_3 \sim (4\bar{\gamma}_3 + 3)n_4$ and $p_3 \sim 4\gamma_3^2 n_1 m_p c^2/3$.

In both cases, the time it takes for the reverse shock to cross a distance dx in the shell material can be given in a similar form up to a constant factor (Kobayashi, Piran, & Sari 1999),

$$\frac{dR}{c} \propto \eta \left(\frac{n_4}{n_1}\right)^{1/2} \frac{dx}{c}, \tag{1}$$

where R is the radius of the shell. Since the motion of the shell is highly relativistic, we can regard R/c as time in laboratory frame.

When a shell is ejected from a source, it has a high density ($n_4 \gg \eta^2 n_1$), so the reverse shock is initially Newtonian. However, as the shell expands, the shell density decreases. There is a possibility that the shock becomes relativistic while it is crossing the shell. Sari & Piran (1995) showed that, using the Sedov length $l = (3E/4\pi n_1 m_p c^2)^{1/3}$, if the shell is thick ($\Delta_0 > l/2\eta^{8/3}$), the reverse shock becomes rela-

tivistic at $R_N = l^{3/2}/\Delta_0^{1/2}\eta^2$ before the crossing at $R_\Delta = l^{3/4}\Delta_0^{1/4}$. If the shell is thin ($\Delta_0 < l/2\eta^{8/3}$), it is dense enough to keep the reverse shock Newtonian. The shock becomes mildly relativistic only when it just crosses the shell at $R_\gamma = l/\eta^{2/3}$.

The total energy of the typical burst can be estimated as $E \sim 10^{52}$ ergs. The ISM density has a typical value of $n \sim 5$ protons cm^{-3}. The thick solid line in Figure 1 separates the thick shell case (*upper right*) and the thin shell case (*lower left*). According to the internal shocks model, the duration of a GRB T is given by the shell width Δ_0/c; the thick shell cases correspond to relatively long bursts.

2.1. *The Thick Shell Case*

In a thick shell case the reverse shock becomes relativistic at R_N and begins to decelerate the shell material. Since the shell density decreases with radius as $n_4 \sim n_1 l^3/\eta^2\Delta_0 R^2$, using equation (1), the number of shocked electrons N_e is proportional to R^2. We obtain the scalings of the hydrodynamic variables in terms of the observer time $t = R/2c\gamma_3^2$,

$$\gamma_3 \sim \left(\frac{l}{\Delta_0}\right)^{3/8}\left(\frac{4t}{T}\right)^{-1/4}, \quad n_3 \sim \frac{8\gamma_3^3 n_1}{\eta} \propto t^{-3/4}, \qquad (2)$$

$$p_3 \sim \frac{4\gamma_3^2 n_1 m_p c^2}{3} \propto t^{-1/2}, \quad N_e \sim N_0 \frac{t}{T}, \qquad (3)$$

where $N_0 = E/\eta m_p c^2$ is the total number of electrons in the shell and $T = \Delta_0/c$ is the time at which the reverse shock crosses the shell. Note that the Lorentz factor γ_3 does not depend on its initial value η after the reverse shock becomes relativistic.

After the shock crosses the shell, the profile of the forward-shocked ISM begins to approach the Blandford-McKee (BM) solution (Kobayashi et al. 1999). Since the shocked shell is located not too far behind the forward shock, it roughly fits the BM solution. Kobayashi & Sari (2000) numerically showed that the evolution is well approximated by the BM solution if the relativistic reverse shock can heat the shell to a relativistic temperature. We apply the BM scalings to the evolution of the shocked shell. The number of the shocked electrons is constant after T because no electron is newly shocked:

$$\gamma_3 \propto t^{-7/16}, \quad n_3 \propto t^{-13/16}, \quad p_3 \propto t^{-13/12}, \quad N = \text{constant}. \qquad (4)$$

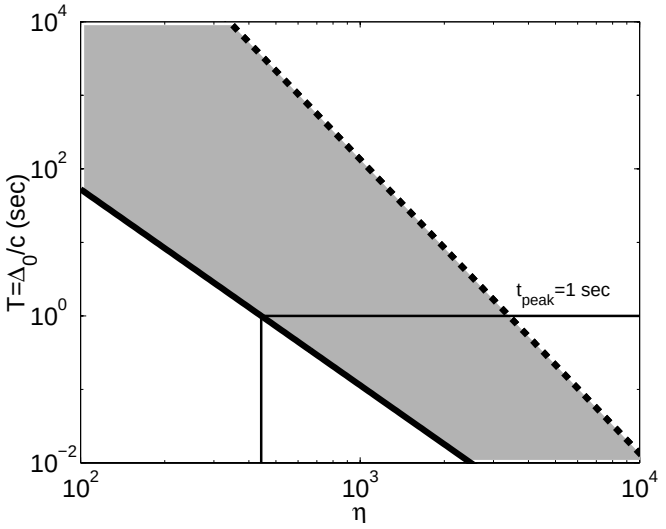

FIG. 1.—Allowed parameter region: the thick solid line separates the thick shell case (*upper right*) and the thin shell case (*lower left*). The slow cooling region for the thick shell case is lower left of the dashed line. That for the thin shell is $\eta < 8 \times 10^4$. The peak time of the reverse shock emission is $t_{\rm peak} = \max(t_\gamma, T)$; the thin solid line depicts $t_{\rm peak} = 1$ s. $E = 10^{52}$ ergs, $n_1 = 5$ protons cm^{-3}, $\epsilon_e = 0.6$, and $\epsilon_b = 0.01$ are assumed.

2.2. *The Thin Shell Case*

In a thin shell case the reverse shock is too weak to decelerate the shell effectively; the Lorentz factor of the shocked shell material is almost constant while the shock propagates in the shell. Because of a slight difference of the velocity inside the shell, the shell begins to spread as $\Delta \sim R/\eta^2$ around $R_s = \eta^2\Delta_0$. Then, the density ratio decreases as $n_4/n_1 \sim (l/R)^3$. In the above thick shell case this spreading effect was not important since it happens after the shock crossing. The scalings before the shock crosses the whole shell at $t_\gamma = l/2c\eta^{8/3}$ are given by

$$\gamma_3 \sim \eta, \quad n_3 \sim 7n_1\eta^2\left(\frac{t}{t_\gamma}\right)^{-3}, \quad p_3 \sim \frac{4\eta^2 n_1 m_p c^2}{3}, \quad N_e \sim N_0\left(\frac{t}{t_\gamma}\right)^{3/2}. \qquad (5)$$

Since the Newtonian reverse shock cannot heat the shell to a relativistic temperature that the BM solution assumes, we are not able to use the BM solution. However, we derived scaling laws for a cold shocked shell, assuming that the Lorentz factor is described by a power law $\propto R^{-g}$ and that the shell expands adiabatically $p_3 \propto n_3^{4/3}$ with a sound speed $\sim(p_3/n_3)^{1/2}$ in the shell's comoving frame. We numerically showed that the scalings with $g \sim 2$ fit the evolution (Kobayashi & Sari 2000):

$$\gamma_3 \propto t^{-2/5}, \quad n_3 \propto t^{-6/7}, \quad p_3 \propto t^{-8/7}, \quad N = \text{constant}. \qquad (6)$$

3. LIGHT CURVES OF THE REVERSE SHOCK EMISSION

We consider now the synchrotron emission from a reverse-shocked shell. The shock accelerates electrons in the shell material into a power-law distribution: $N(\gamma_e)d\gamma_e \propto \gamma_e^{-\hat{p}}d\gamma_e(\gamma_e \geq \gamma_m)$. Assuming that a constant fraction ϵ_e and ϵ_B of the internal energy go into the electrons and the magnetic field, respectively, one finds that the typical random Lorentz factor of the electrons and the magnetic field evolve as $\gamma_m \propto \epsilon_e p_3/n_3$ and $B^2 \propto \epsilon_B p_3$.

The spectrum is given by the broken power laws discussed in Sari, Piran, & Narayan (1998). In this paper we neglect the self-absorption since it does not affect the optical radiation in which we are interested. Then, it has two breaks at the typical synchrotron frequency $\nu_m \propto B\gamma_3\gamma_m^2$ and at the cooling frequency $\nu_c \propto 1/B^3\gamma_3 t^2$, which is the synchrotron frequency of electrons that cool on the dynamical time of the system. The peak flux is obtained at the lower of the two frequencies. Let N_e and D be the total number of the shocked electrons and the distance to the observer, respectively. The observed peak flux density evolves as $F_{\nu,\max} \propto N_e B\gamma_3/D^2$.

The spectra do not depend on the hydrodynamics of the shell. However, the light curve at a fixed frequency depends on the temporal evolution of the break frequencies ν_m and ν_c and the peak power $F_{\nu,\max}$. These depend on how γ_3, n_3, p_3, and N_e scale as a function of t. We will apply the adiabatic evolution discussed in § 2 to the shell evolution. It is justi-

fied if the fraction of the energy going to the electron is small ($\epsilon_e \ll 1$) or if we are in the regime of slow cooling ($\gamma_m < \gamma_c$) where the electrons forming the bulk of the population do not cool.

3.1. *The Thick Shell Case*

A reverse shock crosses a thick shell at $\sim \Delta_0/c$; the peak time of the emission from the reverse shock is comparable to the GRB duration. Using the estimates in § 2, we obtain the break frequencies and the peak flux at the shock crossing time (Sari & Piran 1999a; Waxman & Draine 2000),

$$\nu_m \sim 7.3 \times 10^{14} \epsilon_{e0}^2 \epsilon_{B0}^{1/2} n_{1,5}^{1/2} \eta_{300}^2 \text{ Hz}, \quad (7)$$

$$\nu_c \sim 9.4 \times 10^{15} \epsilon_{B0}^{-3/2} E_{52}^{-1/2} n_{1,5}^{-1} T_{100}^{-1/2} \text{ Hz}, \quad (8)$$

$$F_{\nu,\max} \sim 0.3 D_{28}^{-2} \epsilon_{B0}^{1/2} E_{52}^{5/4} n_{1,5}^{1/4} \eta_{300}^{-1} T_{100}^{-3/4} \text{ Jy}, \quad (9)$$

where we have scaled the parameters as $E_{52} = E/10^{52}$ ergs, $\epsilon_{e0} = \epsilon_e/0.6$, $\epsilon_{B0} = \epsilon_B/0.01$, $n_{1,5} = n_1/5$ cm^{-3}, $\eta_{300} = \eta/300$, $T_{100} = T/100$ s, and $D_{28} = D/10^{28}$ cm. The equipartition values $\epsilon_e = 0.6$, $\epsilon_B = 0.01$, and $n_1 = 5$ protons cm^{-3} are inferred for GRB 970508 (Wijers & Galama 1999; Granot, Piran, & Sari 1999). The scalings before and after the shock crossing at T are

$$t < T: \quad \nu_m = \text{constant}, \quad \nu_c \propto t^{-1}, \quad F_{\nu,\max} \propto t^{1/2}, \quad (10)$$

$$t > T: \quad \nu_m \propto t^{-73/48}, \quad \nu_c \propto t^{1/16}, \quad F_{\nu,\max} \propto t^{-47/48}. \quad (11)$$

It is interesting that ν_m is constant during the shock crossing.

The spectrum is the slow cooling throughout the evolution if $\nu_m < \nu_c$ at T. The shaded region in Figure 1 shows the corresponding parameter region. The flux at a given frequency ν evolves as

$$F_\nu(t < T) \propto \begin{cases} t^{1/2} & \nu < \nu_c, \\ \text{constant} & \nu > \nu_c, \end{cases} \quad (12)$$

$$F_\nu(t > T) \propto \begin{cases} t^{-17/36} & \nu < \nu_m, \\ t^{-(73\hat{p}+21)/96} & \nu_m < \nu < \nu_{\rm cut}, \\ 0 & \nu > \nu_{\rm cut}. \end{cases} \quad (13)$$

The flux at a frequency above ν_c disappears at T because no electron is shocked anymore; this cutoff frequency $\nu_{\rm cut}$ decreases as $\nu_c(T)(t/T)^{-73/48}$ as a result of the adiabatic expansion of the fluid. The index $-(73\hat{p} + 21)/96$ is about -2.1 for the standard choice $\hat{p} = 2.5$.

The light curves are different among three frequency regimes separated by the two frequencies ν_m and ν_c at T. The typical light curves are shown in Figure 2*a*. The flux initially increases at all frequencies as $t^{1/2}$, but the high-frequency light curve flattens when the cooling frequency crosses the given frequency. At T, the flux begins to decay as $t^{-17/36}$ or $t^{-(73\hat{p}+21)/96}$. Finally, it vanishes when $\nu_{\rm cut}$ crosses the given frequency ν at

$$t \sim 700 \epsilon_{B0}^{-72/73} E_{52}^{-24/73} n_{1,5}^{-48/73} T_{100}^{49/73} \times \left(\frac{\nu}{5 \times 10^{14} \text{ Hz}}\right)^{-48/73} \text{s}. \quad (14)$$

For the parameters in the upper right region of the dashed line in Figure 1, the spectrum changes from the slow cooling to the fast cooling during the shock crossing. The light curves are different among three frequency regimes separated by ν_m and ν_c at T. The typical light curves are shown in Figure 2*b*. We neglected the initial slow-cooling phase in the figure since the transition happens at very early time. The flux at a given frequency above ν_c is constant, and below ν_c it increases as $t^{5/6}$. When the shock crosses the shell, above ν_c it vanishes. After that, below ν_c it decreases as $t^{-17/36}$ until $\nu_{\rm cut}$ crosses the given frequency.

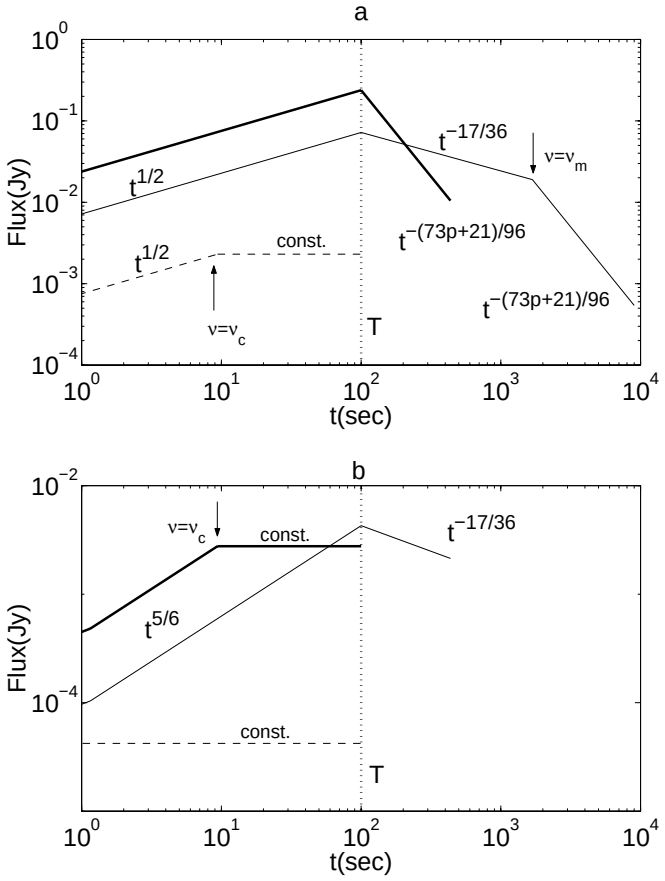

FIG. 2.—Light curves: thick shell case. (*a*) Slow-cooling case: $\eta = 300$; $\nu = 10^{13}$ Hz $< \nu_m(T)$ (*thin solid line*), $\nu_m(T) < \nu = 10^{15}$ Hz $< \nu_c(T)$ (*thick solid line*), and $\nu = 10^{17}$ Hz $> \nu_c(T)$ (*dashed line*). (*b*) Fast cooling case: $\eta = 10^4$; $\nu = 10^{15}$ Hz $< \nu_c(T)$ (*thin solid line*), $\nu_c(T) < \nu = 10^{17}$ Hz $< \nu_m(T)$ (*thick solid line*), and $\nu = 10^{19}$ Hz $> \nu_m(T)$ (*dashed line*). Values of $\nu = \nu_m$ and $\nu = \nu_c$ show the times when the observed frequency ν is crossed by ν_m and ν_c, respectively. $E = 10^{52}$ ergs, $n_1 = 5$ protons cm^{-3}, $\epsilon_e = 0.6$, $\epsilon_b = 0.01$, and $T = 100$ s are assumed.

3.2. *The Thin Shell Case*

As a thin shell case, the shell width Δ_0/c should be smaller than t_γ. Then, separation is expected between the GRB and the peak of the emission. The corresponding parameter region is the lower left of the solid line in Figure 1. The break frequencies and the peak flux at $t_\gamma \sim 3E_{52}^{1/3} n_{1,5}^{-1/3} \eta_{300}^{-8/3}$ s are given by

$$\nu_m(t_\gamma) \sim 9.6 \times 10^{14} \epsilon_{e0}^2 \epsilon_{B0}^{1/2} n_{1,5}^{1/2} \eta_{300}^2 \text{ Hz}, \quad (15)$$

$$\nu_c(t_\gamma) \sim 4.0 \times 10^{16} \epsilon_{B0}^{-3/2} E_{52}^{-2/3} n_{1,5}^{-5/6} \eta_{300}^{4/3} \text{ Hz}, \quad (16)$$

$$F_{\nu,\max}(t_\gamma) \sim 5.2 D_{28}^{-2} \epsilon_{B0}^{1/2} E_{52} n_{1,5}^{1/2} \eta_{300} \text{ Jy}. \quad (17)$$

Note that these do not depend on the value of the initial shell width Δ_0 itself, though Δ_0/c should be smaller than t_γ. The scalings before and after t_γ are as follows:

$$t < t_\gamma: \quad \nu_m \propto t^6, \quad \nu_c \propto t^{-2}, \quad F_{\nu,\max} \propto t^{3/2}, \quad (18)$$

$$t > t_\gamma: \quad \nu_m \propto t^{-54/35}, \quad \nu_c \propto t^{4/35}, \quad F_{\nu,\max} \propto t^{-34/35}. \tag{19}$$

If the spectrum is the slow cooling throughout the evolution, the behavior of the light curves is different among the three frequency regimes separated by ν_m and ν_c at t_γ. Figure 3*a* shows typical light curves. The flux initially increases in all regimes very rapidly as $t^{3\hat{p}-3/2}$ ($\sim t^6$ for $\hat{p} = 2.5$). The slope changes when ν_m or ν_c crosses the given frequency. After t_γ, the flux decays as $t^{-16/35}$ or $t^{-(27\hat{p}+7)/35}$ ($\sim t^{-2.1}$ for $\hat{p} = 2.5$). The emission at a frequency $\nu < \nu_c(t_\gamma)$ disappears when the cutoff frequency crosses it at

$$t \sim 50\epsilon_{B0}^{-35/36} E_{52}^{-8/81} n_{1,5}^{-283/324} \eta_{300}^{-146/81} \times \left(\frac{\nu}{5 \times 10^{14}\ \mathrm{Hz}}\right)^{-35/54} \mathrm{s}. \tag{20}$$

If ν_m is higher than ν_c at t_γ, the spectrum changes from the slow cooling to the fast cooling during the shock crossing. However, it requires a large Lorentz factor $\eta > 8 \times 10^4 \epsilon_{e0}^{-2} \epsilon_{B0}^{-2} E_{52}^{-1} n_{1,5}^{-2}$. Then, the transition happens only if the shell is extremely thin (see Fig. 1), and it is hard to detect such a prompt emission. We show the possible light curves for completeness. The behavior is different among the following four frequency regimes: $\nu < \nu_c(t_\gamma)$, $\nu_c(t_\gamma) < \nu < \nu_0$, $\nu_0 < \nu < \nu_m(t_\gamma)$, and $\nu > \nu_m(t_\gamma)$, where $\nu_0 = \nu_m(t_0) = \nu_c(t_0)$ and t_0 is the transition time from the slow cooling to the fast cooling. The typical light curves are shown in Figure 3*b*, in which the very early slow-cooling phase is neglected.

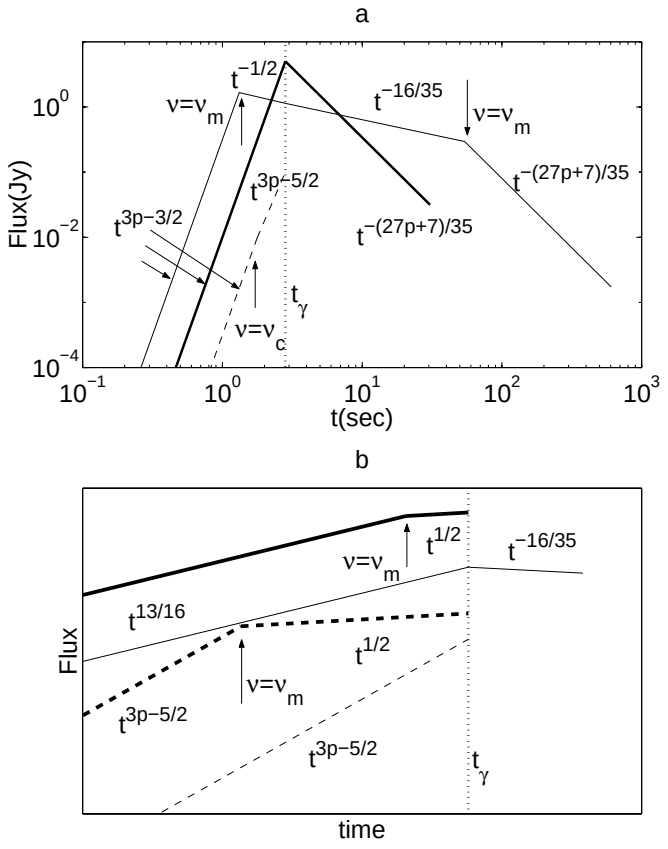

FIG. 3.—Light curve: thin shell case. (*a*) Slow cooling case: $\eta = 300$; $\nu = 10^{13}$ Hz $< \nu_m(t_\gamma)$ (*thin solid line*), $\nu_m(t_\gamma) < \nu = 10^{15}$ Hz $< \nu_c(t_\gamma)$ (*thick solid line*), and $\nu = 10^{17}$ Hz $> \nu_c(t_\gamma)$ (*dashed line*). (*b*) Fast cooling case; $\nu < \nu_c(t_\gamma)$ (*thin solid line*), $\nu_c(t_\gamma) < \nu < \nu_0$ (*thin solid line*), $\nu_0 < \nu < \nu_m(t_\gamma)$ (*thick dashed line*), and $\nu > \nu_m(t_\gamma)$ (*thin dashed line*). Values of $\nu = \nu_m$ and $\nu = \nu_c$ show the time when the observed frequency is crossed by ν_m and ν_c, respectively. $E = 10^{52}$ ergs, $n_1 = 5$ protons cm^{-3}, $\epsilon_e = 0.6$, and $\epsilon_b = 0.01$ are assumed.

4. OBSERVATIONS

In this section we compare our estimates with the ROTSE observations. First, we determine the parameters of the fireball of GRB 990123 from the observations. Then, we make some comments on the lack of the prompt optical emission from GRB 981121 and GRB 991223 in the context of our model.

4.1. *GRB 990123*

GRB 990123 is a very bright burst with a fluence about 100 times that of a median BATSE burst. Absorption lines in the optical afterglow give a lower limit of the redshift $z > 1.6$; the energy required to produce the bright GRB is enormous, $\sim 10^{54}$ ergs for an isotropic emission. ROTSE detected a strong optical flash during the burst (Akerlof et al. 1999). About 50 s after the GRB trigger, it reached a peak of ~ 1 Jy and then decayed with a slope of a power-law index ~ 2.

The fireball of GRB 990123 is likely to be a marginal case (Kobayashi & Sari 2000). However, such a marginal case behaves very much like the thin shell case, since the shell heated by a mildly relativistic shock becomes cold soon. The observed decay is in good agreement with the theory $t^{-2.1}$. This means that the relation among ν_m, ν_c, and the observed optical frequency $\nu_R \sim 5 \times 10^{14}$ Hz is $\nu_m < \nu_R < \nu_c$ at the peak time. Furthermore, the strong optical emission implies that ν_R is close to ν_m (Sari & Piran 1999b).

It is well known that the peak time t_{peak} is sensitive to the Lorentz factor of the shell, so we obtain $\gamma_3 \sim 180 E_{54}^{1/8} n_{1,5}^{-1/8} (t_{\mathrm{peak}}/50\ \mathrm{s})^{-3/8}$. If the reverse shock is mildly relativistic, then the Lorentz factor at the peak time should be close to the initial Lorentz factor, which can be estimated by using equation (20). The last detection of the optical flash by ROTSE was ~ 600 s after the GRB trigger. Using the equality of the Lorentz factors, we obtain $\eta \sim 270$ and $n_1 \sim 0.2$ protons cm^{-3}. With these parameters the typical synchrotron frequency at the peak time is $\sim 1.6 \times 10^{14}$ Hz, which is close to ν_R and is consistent with the initial assumption.

Though we cannot give a strong argument on the raising part of the light curve since the observation is sparse, the power-law index of the slope calculated from the first two ROTSE data is 3.4. The sparseness can make only the index smaller, and the real index is at least larger than that of a thick shell.

4.2. *GRB 981121 and GRB 981223*

The theory succeeded for GRB 990123, but the optical flash was detected only for it so far. Akerlof et al. (2000) reported no detections of the optical flashes to six GRBs with localization errors of 1 deg^2 or better. Especially, GRB 981121 and GRB 981223 are the most sensitive bursts in the sample. If the optical flashes are correlated with the GRB fluences, the optical emission should be more than 2 mag over the ROTSE detection thresholds. The thick lines in Figures 4*a* and 5*a* show the scaled light curves. The GRB fluences f of GRB 981121, GRB 981223, and GRB 990123 in units of 10^{-4} ergs cm^{-2} are 0.07, 0.13, and 1.0, respectively (Akerlof et al. 2000).

GRBs are produced by the internal shocks, while the afterglows and the optical flashes are due to the external

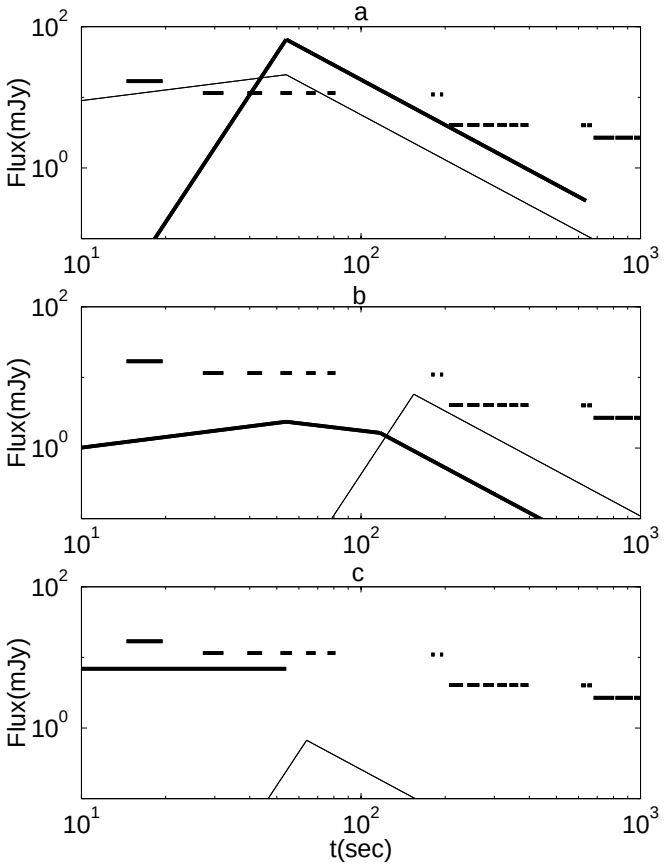

FIG. 4.—GRB 981121: the ROTSE detection thresholds (*segments*) and the theoretical light curves. (*a*) $E = 10^{52}$ ergs (*thin line*) and $E = 10^{54}$ ergs (*thick line*). (*b*) $\eta = 100$ (*thin line*) and $\eta = 1000$ (*thick line*). (c) $n_1 = 10^{-3}$ protons cm^{-3} (*thin line*) and $n_1 = 10^{6}$ protons cm^{-3} (*thick line*). $n_1 = 0.2$ protons cm^{-3}, $\eta = 270$, $E = 10^{52}$ ergs, and $T = 54$ s are used if the values are not specified. The thresholds are calculated assuming that the ROTSE magnitude corresponds to that in the V band.

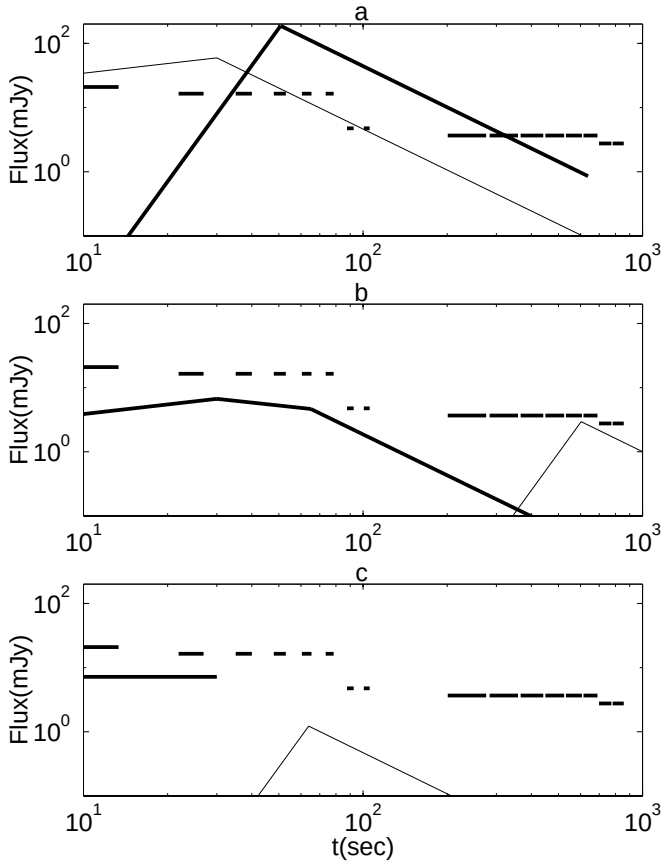

FIG. 5.—GRB 981223: the ROTSE detection thresholds (*segments*) and the theoretical light curves. (*a*) $E = 10^{52}$ ergs (*thin line*) and $E = 10^{54}$ ergs (*thick line*). (*b*) $\eta = 60$ (*thin line*) and $\eta = 1000$ (*thick line*). (*c*) $n_1 = 10^{-3}$ protons cm^{-3} (*thin line*) and $n_1 = 10^{8}$ protons cm^{-3} (*thick line*). $n_1 = 0.2$ protons cm^{-3}, $\eta = 270$, $E = 10^{52}$ ergs, and $T = 30$ s are used if the values are not specified.

shocks. The lack of a direct scaling between the GRB and the afterglow is evidence of the internal shocks model. However, the energy radiated in the GRB phase E_γ is still correlated with the blast-wave energy E estimated from the X-ray afterglow (Freedman & Waxman 1999). According to their analysis, the ratios E_γ/E of 13 events are in between 0.1 and 6, while E_γ ranges from 3×10^{51} to 10^{54} ergs. Furthermore, $E_\gamma/E \sim 3$ of GRB 990123 is a relatively large value in the sample. Therefore, the scaling by the GRB fluence does not overestimate $D^{-2}E$ in general.

GRB 990123 was an exceptionally energetic burst. The energies of GRB 981121 and GRB 981223 should be considerably lower to explain the lower fluences, otherwise the sources are extremely far, $z = 10$ for GRB 981121 and $z = 6.5$ for GRB 981223 assuming $h = 0.5$, $\Omega_0 = 1$, and $\lambda_0 = 0$. Hereafter we assume $E = 10^{52}$ ergs for the two bursts. Since GRB 990123 is a marginal case, a burst with a lower E and a comparable n_1, η, and T is classified into the thick shell case, in which $F_{\nu,\max}$ is proportional to $E^{5/4}$ instead of E. Then, the peak flux for $E = 10^{52}$ ergs is lower by a factor of ~ 3 than that just scaled by the GRB fluence. The thin lines in Figures 4*a* and 5*a* depict the corrected light curves, which are still above the thresholds. The durations of GRB 981121 and GRB 981223 are 54 and 30 s, respectively, and comparable to that of GRB 990123.

A possible solution to the problem is to assume that the reverse shock energy is radiated at a nonoptical frequency, $\nu_m \ll \nu_R$ or $\nu_m \gg \nu_R$. The typical frequency ν_m is proportional to $\epsilon_e^2 \epsilon_B^{1/2} n_1^{1/2} \eta^2$, but the values of ϵ_e and ϵ_B are determined by the microphysics and are likely to be universal. The difference of ν_m should be due to that n_1 and/or η for the bursts deviated from the "canonical" values, $n_1 = 0.2$ protons cm^{-3} and $\eta = 270$.

If n_1 and η are smaller than the canonical values, ν_m is lower than ν_R since $\nu_m \sim \nu_R$ for GRB 990123. Using the normalization by the GRB fluence, the peak flux is

$$F_{\nu_m < \nu_R < \nu_c}(T) \sim 1.0 f_0 E_0^{1/4} T_0^{-3/4} n_0^{\hat{p}/4} \eta_0^{\hat{p}-2} \text{ Jy} , \qquad (21)$$

where the subscript 0 denotes that the parameters are scaled by the values of GRB 990123, $f_0 = f/10^{-4}$ ergs cm^{-2}, $E_0 = E/10^{54}$ ergs, $T_0 = T/50$ s, $n_0 = n/0.2$ protons cm^{-3}, and $\eta_0 = \eta/270$. The fireball is classified into the thin shell case if we assume very small n_1 or η. The dependence of the peak flux on n_1 and η changes to $F_{\nu_R}(t_\gamma) \propto n_0^{(\hat{p}+1)/4} \eta_0^{\hat{p}}$. In Figure 6, F_{ν_R} and $F_{\nu,\max}$ at the peak time are plotted as functions of η or n_1 in the case of GRB 981121. The point at which there are no detections by ROTSE gives upper limits on n_1 and η. Assuming $n_1 = 0.2$ protons cm^{-3}, we get $\eta < 135$ for GRB 981121 and $\eta < 65$ for GRB 981223, or assuming $\eta = 270$, $n_1 < 0.07$ protons cm^{-3} for GRB 981121 and $n_1 < 0.02$ protons cm^{-3} for GRB 981223. The light curves with a low n_1 or η are shown as the thin lines in Figures 4*b*, 4*c*, 5*b*, and 5*c*.

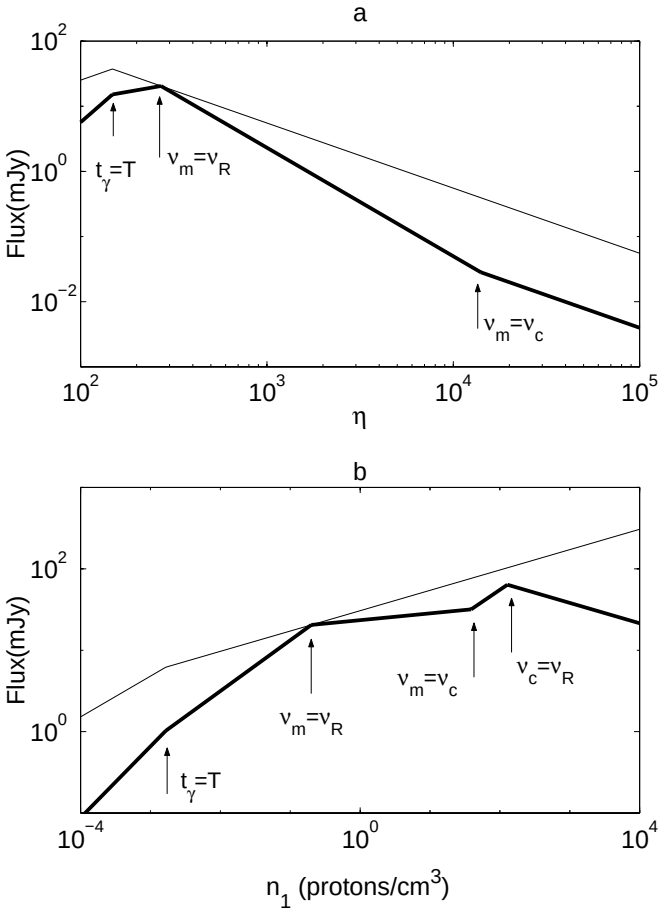

FIG. 6.—GRB 981121: the optical flux F_{ν_R} (*thick line*) and the peak power $F_{\nu,\max}$ (*thin line*) at the peak time max (t_γ, T). $\nu_m = \nu_R$ shows the points for the canonical parameters.

If we assume a larger n_1 or η than the canonical values, the peak flux is given by

$$F_{\nu_R<\nu_m}(T) \sim 1.0 f_0 E_0^{1/4} T_0^{-3/4} n_0^{1/12} \eta_0^{-5/3} \text{ Jy} . \quad (22)$$

The spectrum changes to the fast cooling if n_1 or η is very large. The dependence on n_1 and η changes to $F_{\nu_R} \propto n_0^{7/12}\eta_0^{-1}$. For a larger n_1, ν_c can be lower than ν_R, and then the dependence becomes $n_0^{-1/4}$. The point at which there are no detections gives lower limits, assuming $n_1 = 0.2$ protons cm^{-3}, $\eta > 400$ for GRB 981121 and $\eta > 600$ for GRB 981223, or assuming $\eta = 270$, $n_1 = 2 \times 10^5$ protons cm^{-3} for GRB 981121 and $n_1 = 4 \times 10^6$ protons cm^{-3} for GRB 981223. The light curves for a large n_1 or η are shown as the thick lines in Figures 4*b*, 4*c*, 5*b*, and 5*c*.

A very large ISM density is required to suppress the peak flux, with which the peak power $F_{\nu,\max}$ itself is large (see Fig. 6*b*), thus a large ISM density is an unlikely reason. However, there is a possibility of the extinction. Though we have normalized the optical flux according to the GRB fluence, gamma rays do not suffer any kind of extinction. Half of X-ray afterglow bursts do not have optical afterglows, which might be because of the extinction. The reverse shock radiates at a closer region to the inner engine, which might be crucial. Within the six bursts to which the ROTSE group reported no detections, only the location of GRB 980329 was determined precisely by *BeppoSAX*, and the optical afterglows were observed hours later (Palazzi et al. 1998). However, the ROTSE observation on this burst was not so sensitive. Future observations will provide some additional information to the problem.

5. CONCLUSIONS

We have constructed the full light curves of the reverse shock emission for a short burst (thin shell) and a long burst (thick shell). The typical synchrotron frequency increases rapidly as t^6 in the thin shell case, while it is constant in the thick shell case. For a plausible moderate Lorentz factor, up to a few thousand, the synchrotron spectrum is the slow cooling throughout the evolution, with which spectrum we find that the flux must rise initially steeply as $t^{3\hat{p}-5/2}$ or $t^{3\hat{p}-3/2}$ in the thin shell case and slowly as $t^{1/2}$ in the thick shell case.

The rise ends when the reverse shock crosses the shell. The only exception is the low-frequency emission from a thin shell that already begins to decrease when the rapidly changing typical frequency crosses the observed one. In the decay phase, the light curves are similar for both cases, though the hydrodynamics for each is very different. Then, the detection before the peak should be more useful to give a constraint on the initial properties of the fireball.

The prompt optical emission from GRB 990123 is well described as the reverse shock emission. The observations enabled us to determine the initial Lorentz factor and the ISM density. We found that GRB 990123 is a "luck" burst with the exceptionally large energy and an optimized Lorentz factor to produce a bright optical flash. As the initial Lorentz factor increases, the peak power, $F_{\nu,\max} \propto \gamma_3^2/\eta$, initially rises. However, with a moderate initial Lorentz factor the evolution changes to the thick shell case in which the Lorentz factor at the peak time no longer depends on the initial Lorentz factor. Then, the peak power drops since the number of the electrons in the shell continues to decrease. Therefore, the marginal case gives the brightest optical emission if the typical synchrotron frequency $\nu_m \propto \eta^2$ is close to the optical band. GRB 990123 satisfies the conditions.

The lack of the prompt optical detections by ROTSE for GRB 981121 and GRB 981223 does not give strong constraints on the initial Lorentz factors or the ISM densities. If the Lorentz factor slightly deviates from that of GRB 990123, the peak flux becomes lower than the ROTSE thresholds. It is also possible to explain the nondetections by a lower ISM density.

The author thanks Re'em Sari for helpful discussions and Robert Kehoe for providing the ROTSE data. This work was supported by the Japan Society for the Promotion of Science.

REFERENCES

Akerlof, C. W., et al. 1999, Nature, 398, 400
———. 2000, ApJ, 532, L25
Blandford, R. D., & McKee, C. F. 1976, Phys. Fluids, 19, 1130
Freedman, D. L., & Waxman, E. 1999 (astro-ph/9912214)
Granot, J., Piran, T., & Sari, R. 1999, ApJ, 527, 236
Kobayashi, S., Piran, T., & Sari, R. 1999, ApJ, 513, 669
Kobayashi, S., & Sari, R. 2000, ApJ, 542, 819
Mészaros, P., & Rees, M. J. 1997, ApJ, 476, 231
Palazzi, E., et al. 1998, A&A, 336, L95
Sari, R., & Piran, T. 1995, ApJ, 455, L143
———. 1999a, ApJ, 520, 641
———. 1999b, ApJ, 517, L109
Sari, R., Piran, T., & Narayan, R. 1998, ApJ, 497, L17
Waxman, E., & Draine, B. 2000, ApJ, 537, 796
Wijers, R. A. M. J., & Galama, T. J. 1999, ApJ, 523, 177